Volume 9 | Number 24 | 21 December 2025

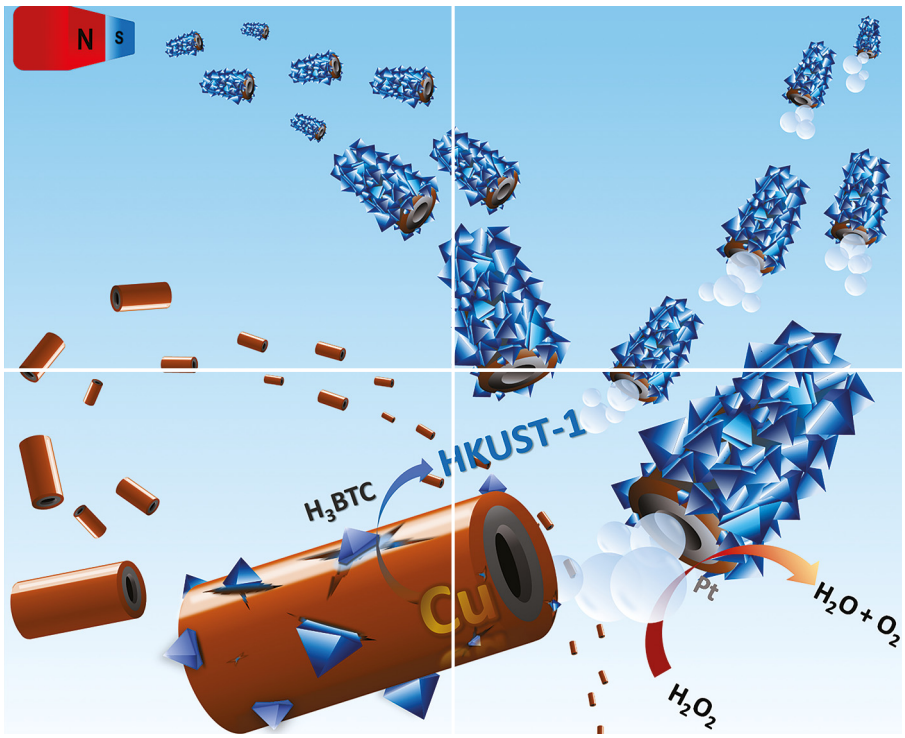

MATERIALS CHEMISTRY

FRONTIERS

CCS 中国化学会 CHINESE CHEMICAL SOCIETY
ICCAS
ROYAL SOCIETY OF CHEMISTRY
rsc.li/frontiers-materials

MATERIALS CHEMISTRY FRONTIERS

RESEARCH ARTICLE

View Article Online
View Journal | View Issue

Cite this: *Mater. Chem. Front.*, 2025, **9**, 3516

Building HKUST-1 metal organic frameworks on a board of Cu tubular micromotors with adaptive propulsive capabilities

Enrique Solano Rodríguez,[a] Beatriz Jurado-Sánchez *[ab] and Alberto Escarpa *[ab]

Received 26th June 2025,
Accepted 23rd August 2025

DOI: 10.1039/d5qm00461f

rsc.li/frontiers-materials

Herein we present one step simplified synthesis of tubular Cu micromotors based on Hong Kong University of Science and Technology (HKUST-1) metal organic frameworks (MOFs). Tubular Cu/Pt, Cu/Ni and Cu/Ni/Pt micromotors prepared *via* template electrodeposition are smartly used as nucleation spots for the synthesis of HKUST-1 MOFs by incubating with the specific ligand, benzene-1,3,5-tricarboxylic acid, without any harsh conditions. The inner engines impart the micromotors with adaptive propulsion mechanisms for future applications: magnetic, catalytic, and hybrid magnetic and catalytic modes, reaching speeds of up to 275 μm s^{-1}. Furthermore, stability studies reveal a delayed degradation of the HKUST-1 MOFs in the micromotors as compared with the free MOFs. The synthesis rationale and delayed stability of the HKUST-1 MOFs in water has been exploited for compound encapsulation and controlled release, as illustrated using fluorescein as the model molecule. This approach has unlocked a new range of possibilities for future applications, offering a promising platform for the development of functional micromotors with improved capabilities.

Introduction

Micromotors (MMs) are microdevices that can convert external energy, such as chemical reactions, light, magnetic fields, or ultrasound, into autonomous movement.[1,2] MMs have become useful tools for a wide range of applications in the bioanalytical,[3] biomedical and environmental fields.[4–6] The advances in this field have brought more and more complex MMs, to satisfy new challenges. On the other hand, metal–organic frameworks (MOFs) are crystalline materials with a periodic network of organic linkers bonded with metal ion nodes to create one-, two, or three-dimensional structures. MOFs have become versatile materials due to their huge number of functional sites and extensive surface area.[7–9]

The coupling between MOFs and MMs has been pursued in recent times due to the value that these kinds of materials can add to these devices.[10,11] Resolving the main problems to achieve success in this task relies on the synthesis and the approach. A first set of strategies explores the functionalization of the MOFs itself with catalytic/magnetic metals engines or enzymes. To this end, zeolitic imidazole[12–14] or University of Oslo (UiO)[15] MOFs were explored. A second convenient strategy for the design of MOF-based micromotors consists of the synthesis of the structure of the MM in the first step. After this process, a post-synthesis MOF surface modification takes place, where the organic linkers and metal nodes of the MOFs and the MMs react under harsh conditions of temperature and/or pH to get an integrated structure.[16–18] Typically, as many steps of synthesis take place, much product is going to be lost. This effect is much more pronounced in the case of MM, due to the small total weight of the product as well as their small size. Furthermore, the yield of surface modification of previously synthesized MMs with MOFs, and the strength of the bond between both structures may not be enough to carry out the pursued tasks.

Inspired by previous MMs works and to solve the above-mentioned challenges, herein we present a new, easy, versatile, and environmentally friendly, simplified, one step synthetic route to synthesize HKUST-1 based MMs using template-prepared Cu/Ni/Pt tubes as precursors for growth of MOFs on boards. Furthermore, we have explored different propulsion mechanisms to achieve a battery of MOF based micromotors depending on the final application: magnetic, catalytic, and both magnetic and catalytic modes. The underlying mechanism behind the synthetic approach adopted here relies on the HKUST-1 MOF structure, which is composed of two Cu ions as metal cores linked with four 1,3,5-benzenetricarboxylate (H_3BTC) ligands.[19] The synthesis of

[a] *Department of Analytical Chemistry, Physical Chemistry, and Chemical Engineering, Universidad de Alcala, Alcala de Henares, E-28802 Madrid, Spain. E-mail: beatriz.jurado@uah.es, alberto.escarpa@uah.es*
[b] *Chemical Research Institute "Andres M. Del Río", Universidad de Alcala, Alcala de Henares, E-28802 Madrid, Spain*

such MOFs has been achieved *via* direct contact of the Cu precursors with H_3BTC acid at room temperature.[20] Such a straightforward route inspired the exploration of new approaches using Cu mesh or nanowires for the preferential growth of HKUST-1 using hydrothermal routes.[21–23] As such, it is possible to select a Cu layer which will react with the organic linker, generating a specific MOF, without any alteration of the other metallic layers thanks to their electrical potential reduction. In this context, we employed a copper metallic microtube as a template to directly grow the HKUST-1 MOF in a single step, achieving a strong MOF–MM coupling that significantly delays material degradation. This elegant MOF-based micromotor synthesis is versatile, accommodating various propulsion strategies—including catalytic, magnetic, and hybrid modes—and exhibits promising capabilities for the encapsulation and subsequent release of target compounds, as demonstrated in the following sections.

Results and discussion

Fig. 1A illustrates the synthesis of Cu@HKUST MMs. MMs have three layers: outer/external, intermediate and internal. The first electrodeposited layer is copper. This layer is the outermost layer and is in direct contact with the medium. In this case, this layer serves as the platform for the synthesis and anchoring of the MOFs. Copper is an ideal metal because it easily reacts with the ligands. This layer provides the Cu metallic ions necessary for building the MOFs. When the external layer is in contact with an organic ligand, oxidation occurs due to the ligand's acidic nature. The resulting oxidized layer provides an ideal environment for the growth of MOFs on its surface. The inner layer enables movement in the device. It can be composed of a single layer of nickel for magnetic propulsion or platinum for catalytic propulsion. If both magnetic and catalytic propulsion are desired, it is important to maintain platinum as the inner layer to ensure internal direct contact with the hydrogen peroxide from the medium, keeping the nickel layer between the copper and the platinum ones.

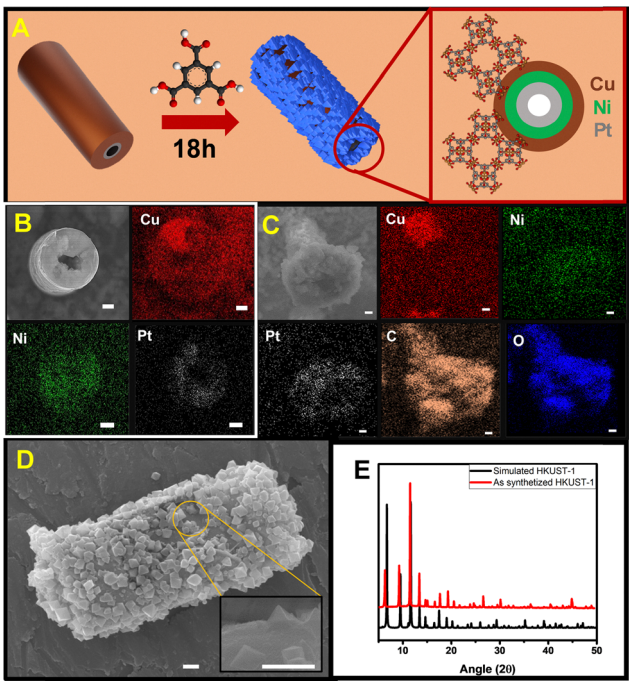

Fig. 1 (A) Schematic of the synthesis of the Cu@HKUST-1/Ni/Pt MMs' adaptive propulsion capabilities using Cu tubular micromotors as precursors of the MOFs. (B) SEM images and elemental mapping of CuNiPt MM and (C) the same MM after the reaction with the organic ligand. (D) SEM image of a MM and zoom on the surface showing the built-in HKUST-1 MOFs. (E) XRD spectra of as-synthetized Cu@HKUST/Ni/Pt MMs and the simulated pattern of HKUST-1. Scale bars, 1 μm.

As a first step, the tubular Cu MMs with different inner engines (Pt, Ni or Pt/Ni) were prepared *via* template electrodeposition as described in the SI, obtaining 207.000 ± 4.000 MMs per membrane (n = 5). As a second step, the MMs were dispersed in 2 mL of H_3BTC alcoholic solution for 18 hours at room temperature, without any harsh or additional conditions. To discuss the uniformity of the resulting MOF MMs, we weighed the MMs before and after the reaction with the organic ligand. In this process, the original weight of MMs increased by ~200%, confirming the appearance of a product, and furthermore, the high relation between these modified MMs and the original MMs (3 : 1). This result, in addition to the SEM images of Fig. 1C and D, can be considered as proof of the homogeneity of the covering by MOF of the original MMs. Under the electrodeposition conditions used, −0.85 V, the only Cu species present in the tubes is Cu^0, without the presence of copper oxides or hydroxides that can contribute to MOF generation.[24] To confirm this statement, X-ray diffraction (XRD) observation of the Cu tubes was conducted. As can be seen in Fig. S1, the pattern indicates the main presence of Cu^0.[25] Some traces of Cu_2O are also observed, but we attributed this to the tube oxidation *via* the effect of exposition to air, as the sample needs to be dried to perform measurements. As such, HKUST-1 synthesis can be explained by the generation of porous supramolecular structures by H_3BTC on the Cu surface of the MMs. This results in the generation of a paddlewheel, HKUST-1, which consists of deprotonated H_3BTC, resulting in the oxidation of Cu^0 to Cu^{2+}. Such nucleation points initiate the generation of the MOFs over the MM surface. See Fig. S2 for a detailed synthesis scheme and mechanism. Please note here that the reaction is performed under room temperature conditions, where oxygen can contribute as an ionization agent for Cu and deprotonation agent for the ligand.[26,27]

The choice of trimesic acid as the ligand is not trivial. While zeolitic imidazole (ZIF-8) and University of Oslo (UiO-66) MOFs have been extensively studied and synthetized by simplified routes, they have certain limitations compared with our specific synthesis approach, which relies on controlled nucleation at the surface of the micromotor external metal layer. In this context, the role of the HKUST-1 organic ligand (trimesic acid) is crucial. Its acidic nature activates the metal surface, enabling the growth of the MOFs. ZIF-8 was initially considered for this purpose; however, its ligands were not suitable for initiating metal surface activation, which prevented the formation of a

strong MOF–metal interface. To strengthen and investigate this strategy involving acidic ligands, we used other acidic ligands that could effectively attack the metal surface. We successfully synthesized MOFs–metal–metal systems using fumaric acid, a linear dicarboxylic acid, as demonstrated in the SI (see Fig. S3). On the other hand, both terephthalic acid, the linker in UiO-66, and trimesic acid, used in HKUST-1, belong to the benzoic acid family. Terephthalic acid has two carboxylic groups in the 1,4 positions, and trimesic acid has three in the 1,3,5 positions. However, terephthalic acid is only slightly soluble in ethanol, unlike trimesic acid, which is significantly more soluble. For this reason, we selected trimesic acid, which enables a more straightforward and reproducible synthesis.

The morphology and element composition of the Cu/Ni/Pt (Fig. 1B) and Cu@HKUST/Ni/Pt MMs (Fig. 1C) was studied by SEM and EDX mapping. The MMs showed a cylindrical shape, with a plane surface and a space in the center. EDX mapping revealed a concentric structure composed of an outer layer of copper, and after it, different metals, Ni, Pt, or both Ni-Pt. Regarding MOF-MM, morphological changes are evident, octahedral structures appear all along the surface which are mainly composed of carbon and oxygen. As can be seen, the entire surface of the MMs has been covered with plenty of octahedral structures, growing from the copper layer itself (see also the inset for an amplified view and the typical morphology of the HKUST-1 MOF) (see Fig. 1D). The XRD spectra of Fig. 1E further reveals the typical pattern diffraction of as-synthetized Cu@HKUST/Ni/Pt fitting with the simulated one. Please note that the experimental XRD pattern shows a slight displacement of the angle where the diffraction peaks appear, probably due to the presence of solvent in the structure, modifying the size of the unit cell and consequently, causing a slight displacement of the diffraction angle. At the same time, MMs were observed under SEM microscopy, to check if their surfaces had been covered with the MOF (Fig. 1D). Table S1 shows relevant information explaining different ways of synthesis of MOF-based micromotors using the post MOF-integration-in-micromotor synthesis approach. As can be seen, all the examples involve more steps than those proposed in this work. Furthermore, they mostly use high temperatures, hydrothermal methods or both. In addition, the time needed to achieve the final chemical coupling MM-MOF is in all cases higher than that in our proposed method. So, in conclusion, we have successfully tried to simplify the synthesis of these microdevices, creating a very versatile method, cheap, quick and environmentally friendly, getting very good results with the additional advantage of the strong bond between MOF and MM, essential to guaranteeing good development of the task in root-like behavior magnetic motion for controlled release applications, as will be demonstrated in the following discussion.

After the successful synthesis of the Cu@HKUST-1/Ni/Pt MMs, we tested the propulsion abilities for future applications, using tap water instead of deionized water as realistic media to test potential effects on MMs stability and the role in the propulsion. As can be seen in the schematic pictures of Fig. 2A, pioneering evaluation of catalytic, magnetic, and both catalytic and magnetic

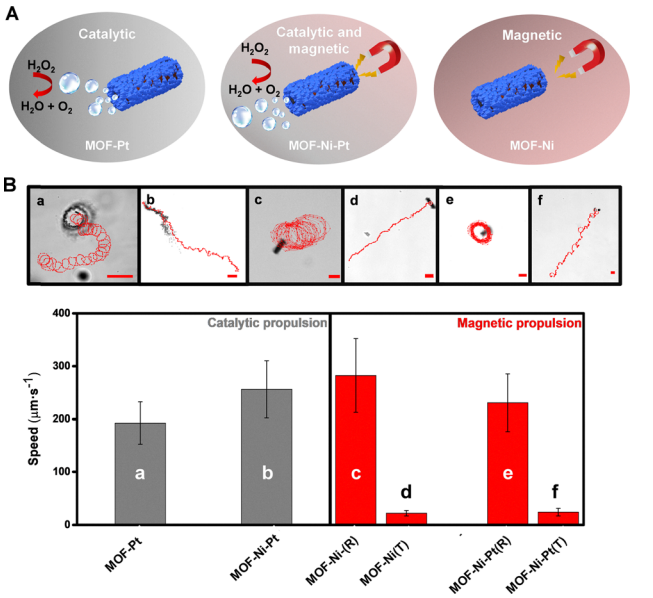

Fig. 2 (A) Schematic of the propulsion modes of the Cu@HKUST-1/Ni/Pt MMs. (B) Time-lapse images (Taken from Videos S1 and S2) and corresponding speeds of the Cu@HKUST-1/Ni/Pt MMs according to the propulsion mechanism ((a) and (b) for catalytic propulsion and (c–f) to magnetic propulsion: (c) and (e) under 3.5 V spin magnet, only rotational) and (d) and (f) under both spin magnet and 1 V electromagnetic magnet, rotational and translational. Scale bars, 1 μm. Conditions: 2.5% H_2O_2, 5% of Tween 20 as the surfactant.

modes was made in comparison with the other approaches listed in Table S1. Details of video recording are listed in the SI. Magnetic propulsion was achieved with a tailored magnetic device integrating four electromagnets, as described in the experimental section of the SI. For the catalytic propulsion mode, speeds are very similar between Pt and Ni–Pt based MMs around 200–250 μm s^{-1}. In fact, a slightly higher speed in the magneto-catalytic propulsion mode, due to the synergic effect of magnetic and catalytic propulsion, which also proves that an additional metallic layer and its weight do not have a remarkable effect on the propulsion.[28,29] For magnetic propulsion (see Fig. 2B, right), different speeds can be measured: rotational and translational. The first one depends on the rotation of the electromagnetic system, being able to convert the angular speed to linear speed thanks to the relation $v = w \cdot r$, where "w" expresses the angular speed (rad s^{-1}) and "r" expresses the radium (μm). MOF-Ni and MOF-Ni-Pt MM show very similar speed values, around 225–275 μm s^{-1}. The second one, much lower than the previous one, around 25 μm s^{-1}, shows the speed of the MMs because of the combined effect of rotation and translational dragging towards one specific electromagnet in a straight line. In both cases, these speeds are very similar between Ni and Ni–Pt based MMs, so again the additional weight of a third layer seems not to have any remarkable consequence. Interestingly, all in all, these data reflect the successful MM modification with the HKUST-1 MOFs, maintaining further functionality in terms of propulsion for future applications.

Next, we carried out a physical–chemical study of the HKUST-1 and Cu@HKUST/Ni/Pt MM stability. Indeed, it is

well-known that this MOFs is specially affected by water. The strong interaction between water molecules and the paddle-wheel Cu(II) sites results in the irreversible degradation of the MOF.[30–32] As MM applications are realized in aqueous media (even biological), it is important to study the effect of water on the stability of the Cu@HKUST-1/Ni/Pt MMs. To this end, initially, single copper layer micromotors were synthesized and left to react entirely with the organic ligand for a few days, assuring that all the MM surface is covered with the HKUST-1 MOFs, completely covering the supporting metallic copper structure. First, the HKUST-1 MOF resistance to water was tested. A certain amount of this pure HKUST-1 MOFs was put into a 20 mL vial with deionized water, showing a dark blue sand-like aspect (Fig. 3A(a)). After 3 hours, the deep-blue dispersion turned into a light-blue one, changing even the appearance of the HKUST-1, from small dots to a thread-like shape. After 24 hours, the HKUST-1 MOF was totally converted into a light-blue mass (Fig. 3A(b)). To understand the internal effect of the water degradation on the structure, XRD, SEM, FTIR and BET analyses were carried out. The XRD pattern (Fig. 3a) reveals different peaks between MOF 0 h (1) and MOF 24 h (2) in water, indicating a change in the crystalline structure, which can even be noticed in the SEM images of HKUST-1 before (octahedral shapes) and after (tape-like shapes) the contact with water. FTIR analysis was carried out in both samples, at 0 hours and 24 hours in water (Fig. 3B). The FTIR spectra shows different signals between as-synthetized HKUST-1 and HKUST-1 after 24 hours in water, due to substitution of the ligand by water molecules, as is reported in the bibliography. In the pristine HKUST-1, 750–770 cm^{-1} signals are attributed to Cu–O bonds. 1370 cm^{-1} is the C–O bond of the trimesic acid, and 1448 and 1550 cm^{-1} signals are due to the C═O bond of the ligand. The 1649 cm^{-1} signal is attributed to C═C from the aromatic ring. On the other hand, HKUST-1 exposed to water shows a difference in the region of the C═O, with two new signals appearing at 1480–1510 cm^{-1}, a new one appearing in the C–O region at 1092 cm^{-1} and the 1045 and 1115 cm^{-1} signals almost disappearing. These changes can be explained as being due to the rupture of the COO–Cu bond, leaving a free COO–, which modifies the vibration frequency. This substitution is the cause for the change in the pore size, opening the space because of the destruction of the original bond between the ligand and the metallic atom. A detailed FITR analysis at different times can be found in Fig. S3. As can be seen, the spectrum changes after three hours due to the destruction of the network by water. The 1030–1100 cm^{-1} signals, which are associated with the carboxylate group linked to the copper, change to give a new signal at 1090 cm^{-1}, indicating a change in the surrounding of this group due to the rupture of the copper–carboxyl bond. The same conclusion can be drawn from the main single signal at 1370 cm^{-1} which is associated with the C–O bond of the carboxylic group. This signal splits into two smaller signals at 1380–1360 cm^{-1}. This change can be explained as being due to the transition from coordinated to non-coordinated carboxylates to copper. The aromatic region, 1600–1400 cm^{-1}, shows a change probably due to the partial protonation and solubilization of the organic ligand, beginning at three hours. BET analysis shows this change as a decrease of the pore size, from 60 to 31 Å and, in consequence, the decrease of the surface area from 2097 m^2 to 26 m^2. Fig. 3c displays the differences between the as-synthetized HKUST-1 MOFs and the degraded one.

In turn, the stability of HKUST-1 MOFs MM was also studied. For this purpose, XRD diffractions were taken at different times in contact with water, 0 h, 20 minutes, 1 h, 3 h, 8 h, 12 h, and 24 h. As can be seen in the SEM images and XRD spectra of Fig. 4, the free HKUST-1 MOF maintains its crystalline structure forup to 1 hour,[19,33] the time when different new peaks begin to appear. After this time, the HKUST-1 MOF gradually changes until a totally different XRD diffraction pattern at 24 hours of water contact is seen (Fig. 4B(a)). On the other hand, Fig. 4B(b) displays the diffraction pattern of Cu@HKUST-1/Ni/Pt MMs (please note that due to the small amount in weight of MMs it is very hard to get a very resolved diffraction pattern). Yet, the main peaks are maintained between pure HKUST-1 MOFs and Cu@HKUST-1/Ni/Pt MMs, but the latter presents a much higher signal-to-noise ratio and other different peaks from the pure copper layer. Very interestingly, HKUST-1 peaks appear even after 24 hours of water contact. This fact can be explained by the specific degradation mechanism of HKUST-1 MOFs. Water triggers a break between the copper atom and the organic ligand.[30] This hydrolysis brings consequently an increase of H_3BTC in the vicinity of the MMs, but, in contrast with the free MOF situation, now the HKUST-1 destruction leaves a raw copper layer ready to react again with a certain amount of this free ligand. This process can delay the total disappearance of the HKUST-1 MOFs and justify why their peaks are present for up to 24 hours in contact with water. But this does not imply a very high-water stability of MOF-MM as can be seen in SEM images of Fig. 4. A MM at 0 h in water is covered with plenty of MOFs. After 24 hours, it is still

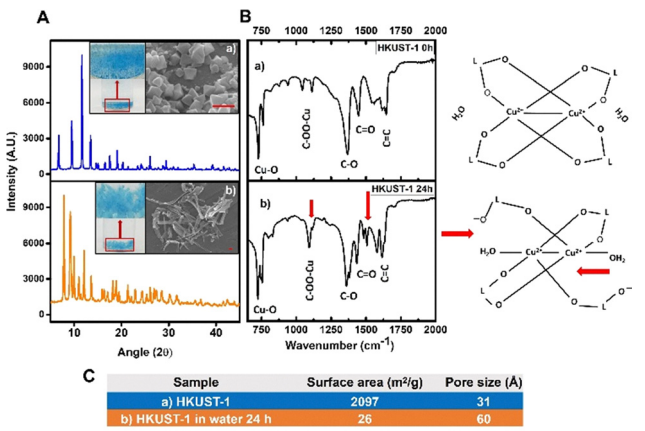

Sample	Surface area (m^2/g)	Pore size (Å)
a) HKUST-1	2097	31
b) HKUST-1 in water 24 h	26	60

Fig. 3 Stability of HKUST-1 (A) XRD, optical images and SEM images of as-synthetized HKUST-1 (1) and HKUST-1 after 24 hours in water (2). Scale bars: 1 μm. (B) FITR of as-synthetized HKUST-1 and a schematic structure of the material before the ligand substitution by water (1), and HKUST-1 after 24 hours in water and a schematic structure of the material after the water attack (2). (C) Surface area and pore size of as-synthetized HKUST-1 and HKUST-1 after 24 hours in water.

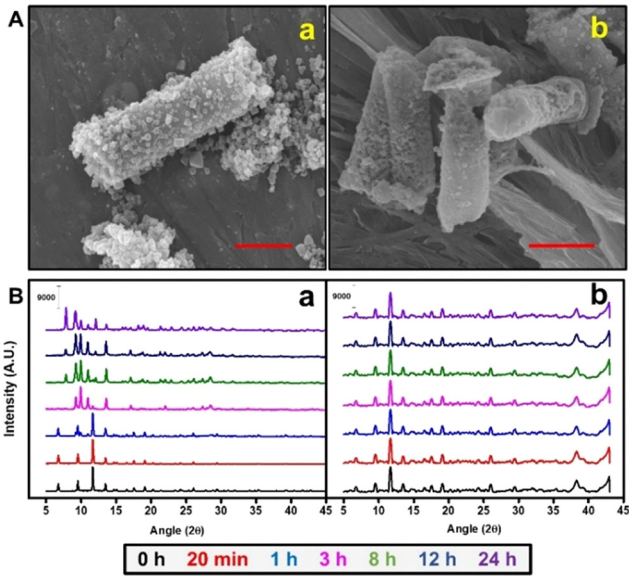

Fig. 4 Stability of Cu@HKUST MMs (A) SEM images of Cu@HKUST-1/Ni/Pt MMs at 0 h (a) and 24 h in water (b). (B) X-ray diffraction patterns of free HKUST-1 (a) and HKUST-1 in direct contact with the surface of the MMs (b) at different times. Scale bars 5 μm.

possible to distinguish some octahedral structures, but tape-like figures indicating the degraded MOFs are everywhere. The MOF is gradually destroyed, and after 24 hours, octahedral structures can be barely observed. Probably, the HKUST-1 structure is much more detected in the diffraction patterns than in the destroyed MOF because the latter has lower crystallinity in comparison with the first one. So, in conclusion, the HKUST-1 degradation process in water on boards of MMs is delayed.

The HKUST-1 degradation, instead of being a problem, can be converted into an advantage, releasing to the medium different compounds of interest previously loaded. To test this possible application, a model fluorescent molecule, fluorescein was chosen. To load it, a 0.025 M solution of this fluorophore was added to an alcoholic solution of H_3BTC. Cu/Ni MMs were then added to this solution and allowed to react for 24 hours. The resulting product was collected using a magnet and cleaned with absolute ethanol several times. After this process, the fluorescein loaded Cu@HKUST-1/Ni MMs were tested by putting them in contact with water and guided using an electromagnetic system. As can be seen in Fig. 5 A, no apparent fluorescence is observed in control experiments with Cu/Ni MMs (parts 1 and 2), unloaded Cu@HKUST-1/Ni MMs (parts 3 and 4), as compared with the bright fluorescence in the surface of the loaded Cu@HKUST-1/Ni MMs (parts 5 and 6). After 24 hours in water, only a minimum fraction of this fluorescence can be perceived in the fluorescein-loaded Cu@HKUST-1/Ni MMs surface, the rest of it being transferred to the water solution (see parts 7 and 8). This is also reflected in the time lapse-images of Fig. 5 and corresponding Video S3, which shows the real-time release of the fluorescein cargo, with a clearly distinguished trail coming out of the MMs.

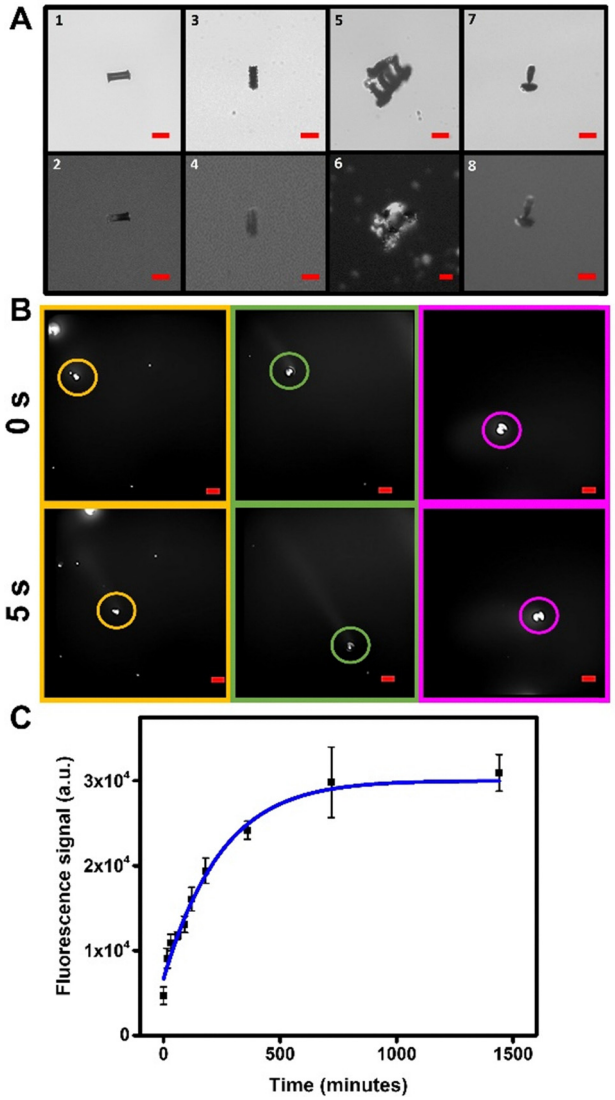

Fig. 5 (A) Micrographs of Cu@HKUST-1/Ni MMs in different steps of the synthesis with bright-field image (upper) and fluorescence image (lower): as-synthetized Cu/Ni MMs (1 and 2), unloaded Cu@HKUST-1/Ni MMs (3 and 4), fluorescein loaded Cu@HKUST-1 (5 and 6) and fluorescein loaded Cu@HKUST-1/Ni MMs after 24 hours in water (7 and 8). (B) Time-lapse images (over 5 s period, taken from Video S3) showing the release of the fluorescein cargo in water. Scale bars: 20 μm. Conditions: Applied voltage, 1 V, GA-2A filter, λ_{ex} 510–560 nm. (C) Release profile of fluorescein in water for 24 hours. Conditions: λ_{ex} 475 nm and λ_{em} 520–625 nm. Error bars represent the mean values ± standard deviation (n = 3).

The fluorescein release process was monitored to know the releasing profile. To this end, supernatant fluorescence was measured for 24 hours. As it can be seen in Fig. 5 C, the release follows an asymptotic tendency, delivering in the first term all the external cargo of the outer part of the MOF, and with the beginning of its degradation, the inner cargo its gradually released to the medium until its stabilization at 12 hours. As a result of this process, it can be said that the cargo has been successfully released, due to the degradation and self-destruction in contact with water of the HKUST-1 on the MM surface.

In this regard, and with the aim of further investigating the release process, we performed control experiments by incubating Cu/Ni MMs and Cu@HKUST-1/Ni MMs with fluorescein and Cu/Ni MMs incubated with the ligand and fluorescein. As a blank, we used Cu@HKUST-1/Ni without any contact with fluorescein. Fig. S5, A shows that Cu@HKUST-1/Ni MMs exhibit no intrinsic fluorescence. For comparison, Cu/Ni MMs incubated with fluorescein display slight fluorescence, likely due to nonspecific adsorption of molecules in the inner part of the MM tube, where solvents in the cleaning phase have limited access. When the Cu@HKUST-1/Ni are first coated with HKUST-1 and subsequently incubated with fluorescein, noticeable adsorption of the cargo occurs on the MOF surface. However, adding fluorescein together with the organic ligand during HKUST-1-MM formation allows for the simultaneous growth and encapsulation processes to fully utilize the MOF's porous structure. This increases the cargo release by four times compared to the previous method. The potential use of the Cu@HKUST-1/Ni as a drug-delivery system in biological environments is supported by their cytotoxicity. An MTT assay with HeLa cells was carried out at different concentrations of MOF Ni-MMs, being able to hold 10.000 MM per mL without remarkable cytotoxicity (Fig. S5B).

Conclusions

We have developed a new family of MMs, based on HKUST-1 MOFs, with adaptive propulsion modes: magnetic, catalytic, and both magnetic and catalytic; with simplified synthesis and delayed degradation. This pioneering coupling MM-MOF can be easily synthesized at room temperature, resulting in total coverage of HKUST-1 MMs in just 18 hours. Furthermore, we have tested the behavior of these MMs in water, showing a slowed-down degradation in comparison with the free MOFs, allowing applications related to the controlled cargo delivery, as has been demonstrated with the release of a fluorescence model molecule. These findings, related to the synthetic rationale and delayed stability, open new avenues in MM chemistry, highlighting their potential for future applications in the bioanalytical, biomedical, and environmental fields. Moreover, it allows further expansion of the applications of MOFs, since the MOFs-MM coupling is not yet widely explored. Advances are also expected in applications of MOFs where MMs play a key role due to their inherent propulsion and are essential in biomedicine such as drug-delivery in tissues and organ-on-chip systems. While we have successfully demonstrated significant advancements in HKUST-1 MOF-based micromotors, there are some potential shortcomings or areas that might require further investigation, which are common challenges in this field: long-term stability in complex environments over extended periods for practical applications; biocompatibility and potential toxicity of the micromotor components (Cu, Pt, Ni, and the MOF itself, especially its degradation products); scalability of synthesis for mass production, which is also limited by the cost of some materials; sophisticated control and targeted specificity over degradation/release. Surely, the transition from proof-of-concept to real-world applications involves overcoming such challenges.

Experimental section

Reagents and materials

Copper sulfate (cat. 209198), trimesic acid (H_3BTC) (cat. 482749), nickel(II) chloride (cat. N6136), chloroplatinic acid (cat. 520896) and Tween 20 (cat. P9416) were purchased from Sigma-Aldrich. Boric acid (cat. 180570010) was supplied by Thermofisher. Absolute ethanol (cat. ET0005005P), isopropanol (cat. AL03102500) and dichloromethane (cat. CL3352500) were supplied by Scharlau (Spain). Membranes of 5 μm in diameter were purchased from Whatman (cat. 7060-2513).

Equipment

An Autolab potentiostat model PGSTAT101 was used for Cu micromotor electrodeposition. Membranes were coated with a ~50 nm gold layer by sputter coating. Scanning electronic microscopy (SEM) images were taken using a JEOL JSM-IT500 and JEOL JSM 6335-F coupled to an energy ray-dispersive detector. A Nikon Eclipse Ti-2 inverted optical microscope coupled to a PCO Panda camera was used to take images and to record videos. XRD diffraction patterns were obtained with a Bruker D8 Advance A25 diffractometer from the X-ray unit at the Complutense University of Madrid. BET analysis was carried out using the porous solid analysis unit of the University of Malaga (UMA). FTIR spectrums were obtained with an Agilent Cary 630, collecting 16 scans with a resolution of 4 cm^{-1}. Finally, for the fluorescence intensity, one batch of MOF-MM grown in the presence of fluorescein was added to a 5 ml of deionized water. 150 μL were taken three times and measured in a lector reader model Biotek citation 5, with λ_{ex} 475 nm and λ_{em} 520–625 nm.

Template electrosynthesis and metal–organic framework growth on the micromotors

For the electrodeposition, the gold-supper membrane was assembled in a tailored electrochemical cell using an Ag/AgCl reference electrode and a Pt wire as the counter electrode. The outer Cu layer was synthetized from a plating solution containing 0.15 M of $CuSO_4{\cdot}5H_2O$ in 0.015 M H_2SO_4 by applying a −0.85 V voltage for 200 seconds. For the synthesis of Cu–Pt micromotors, the Pt layer was electrodeposited from a 4 mM $H_2PtCl_6{\cdot}(H_2O)_6$ solution in 0.5 M boric acid, which was subjected to an amperometric process (−0.4 V for 750 s). For the synthesis of Cu–Ni micromotors, a 0.5 M $NiCl_2$ solution in 0.1 M HCl was subjected to −1 V for 120 seconds. Finally, for Cu–Ni–Pt micromotors synthesis, the same process was carried out, only decreasing Ni electrodeposition time from 120 to 80 seconds. After the electrodeposition process, the gold layer of the membrane was removed and rubbed with alumina powder and water. To release the micromotors, the polished polycarbonate membrane was immersed into 2 mL of dichloromethane and shaken for one hour. Micromotors were collected *via* centrifugation, taking out the supernatant. This process was repeated with isopropanol and finally with absolute ethanol. Once the micromotors were totally released from the membrane and cleaned, 2 mL of H_3BTC alcoholic solution was added and allowed to react for 18 hours

at room temperature. After this time, a blue color appears in the H_3BTC solution. Micromotors were next isolated *via* centrifugation (3 minutes, 3000 rpm) and cleaned with absolute ethanol. This process was repeated three times.

Micromotor propulsion

For catalytic and magneto-catalytic propulsion, videos were recorded by placing 1 μL of micromotor solution, 1 μL of hydrogen peroxide (final concentration, 2.5%), 1 μL of Tween 20 (final concentration, 5%) and 1 μL of tap water in a glass slide placed on top of the optical microscope. Videos were taken using the 20× objective at 40 frames per second. The speed was analyzed using NIS-tracking software. For magnetic propulsion, a custom-design electromagnetic system was used. The magnetic module consisted of a 3D printed platform tailored to fit the plate of the microscope stage, with four tilted cylindrical holders accommodating, a holder for permanent magnets setup, and an opening to accommodate the microscope slide. Four magnets (0.05–10.5 V) and Heschen electromagnet solenoids (P30/22, 30 mm, 12 V or P50/27, 50 mm, 24 V) were used. Arduino IDE 1.9 was used to develop a program to control the Arduino Nano board. An Arduino Nano board was used to switch the relays on demand and the serial port of the microcontroller was used as a user interface to input the commands corresponding to the desired magnetic gradient direction. To perform the experiments, the rotating field was fixed at a constant speed by fixing the applied voltage to 1 V.

Author contributions

E. Solano Rodríguez: conceptualization, data curation, formal analysis, investigation, visualization, writing – original draft, writing – review & editing. B. Jurado-Sánchez: conceptualization, data curation, formal analysis, visualization, funding acquisition, project administration, resources, supervision, writing – original draft, writing – review & editing. A. Escarpa: conceptualization, formal analysis, funding acquisition, project administration, resources, supervision, writing – review & editing. The manuscript was written through contributions of all authors. All authors have given approval to the final version of the manuscript.

Conflicts of interest

There are no conflicts to declare.

Data availability

Data for the article are available upon reasonable request to the authors due to confidentiality requirements. The data supporting this article have been included as part of the SI. Supplementary information: Fig. S1, S2 and Videos S1–S3. See DOI: **https://doi.org/10.1039/d5qm00461f**.

Acknowledgements

This work was supported by the Spanish Ministry of Science, Innovation and Universities [Grant PID2020-118154GB-I00 funded by MCIN/AEI/10.13039/501100011033 (A. E., B. J-S.), grant PID2023-152298NB-I00 funded by MCIN/AEI/10.13039/501100011033 and FEDER, UE (A. E., B. J. S.); grant TED2021-132720B-I00, funded by MCIN/AEI/10.13039/501100011033 and the European Union "NextGenerationEU"/PRTR (A. E., B. J-S.); grant CNS2023-144653 funded by MCIN/AEI/10.13039/501100011033 and the European Union "NextGenerationEU"/PRTR (B. J-S.); and FPI contract PRE2021-099801, (E. S.)]; the Community of Madrid [grant number CM/JIN/2021-012 (B. J-S.)], Junta de Comunidades de Castilla la Mancha [grant number SBPLY/23/180225/000058 and FEDER] and the Universidad de Alcalá [Línea de Actuación Excelencia para el Profesorado Universitario de la UAH, EPU-INV-UAH/2022/003 (B. J-S.)].

References

1 G. A. Ozin, I. Manners, S. Fournier-Bidoz and A. Arsenault, Dream nanomachines, *Adv. Mater.*, 2005, **17**, 3011–3018.
2 E. Karshalev, B. Esteban-Fernández de Ávila and J. Wang, Micromotors for "Chemistry-on-the-Fly", *J. Am. Chem. Soc.*, 2018, **140**, 3810–3820.
3 A. Escarpa and B. Jurado-Sánchez, Micromotors meet collective (bio)sensing: the asset behind the assay, *Anal. Chem.*, 2025, **97**, 12913–12924.
4 C. Chen, S. Ding and J. Wang, Materials consideration for the design, fabrication and operation of microscale robots, *Nat. Rev. Mater.*, 2024, **9**, 159–172.
5 J. Wang, Z. Xiong, J. Zheng, X. Zhan and J. Tang, Light-driven micro/nanomotor for promising biomedical tools: principle, challenge, and prospect, *Acc. Chem. Res.*, 2018, **51**, 1957–1965.
6 T. Patino, A. Porchetta, A. Jannasch, A. Lladó, T. Stumpp, E. Schäffer, F. Ricci and S. Sánchez, Self-sensing enzyme-powered micromotors equipped with pH-responsive DNA nanoswitches, *Nano Lett.*, 2019, **19**, 3440–3447.
7 H. Furukawa, K. E. Cordova, M. O'Keeffe and O. M. Yaghi, The chemistry and applications of metal-organic frameworks, *Science*, 2013, **341**, 1230444.
8 C. R. Kim, T. Uemura and S. Kitagawa, Inorganic nanoparticles in porous coordination polymers, *Chem. Soc. Rev.*, 2016, **45**, 3828–3845.
9 W. Wang, D. Chen, F. Li, X. Xiao and Q. Xu, Metal-organic-framework-based materials as platforms for energy applications, *Chem*, 2024, **10**, 86–133.
10 A. Terzopoulou, J. D. Nicholas, X.-Z. Chen, B. J. Nelson, S. Pané and J. Puigmartí-Luis, Metal–organic frameworks in motion, *Chem. Rev.*, 2020, **120**, 11175–11193.
11 J. Bujalance-Fernández, B. Jurado-Sánchez and A. Escarpa, The rise of metal–organic framework based micromotors, *Chem. Commun.*, 2023, **59**, 10464–10475.
12 A. Ayala, C. Carbonell, I. Imaz and D. Maspoch, Introducing asymmetric functionality into MOFs via the generation of

metallic Janus MOF particles, *Chem. Commun.*, 2016, **52**, 5096–5099.

13 T. T. Y. Tan, J. T. M. Cham, M. R. Reithofer, T. S. Andy Hor and J. M. Chin, Motorized Janus metal organic framework crystals, *Chem. Commun.*, 2014, **50**, 15175–15178.

14 Y. Yang, X. Arqué, T. Patiño, V. Guillerm, P.-R. Blersch, J. Pérez-Carvajal, I. Imaz, D. Maspoch and S. Sánchez, Enzyme-powered porous micromotors built from a hierarchical micro- and mesoporous UiO-Type metal–organic framework, *J. Am. Chem. Soc.*, 2020, **142**, 20962–20967.

15 J. Li, X. Yu, M. Xu, W. Liu, E. Sandraz, H. Lan, J. Wang and S. M. Cohen, Metal–organic frameworks as micromotors with tunable engines and brakes, *J. Am. Chem. Soc.*, 2017, **139**, 611–614.

16 X. Wang, X.-Z. Chen, C. C. J. Alcântara, S. Sevim, M. Hoop, A. Terzopoulou, C. de Marco, C. Hu, A. J. de Mello, P. Falcaro, S. Furukawa, B. J. Nelson, J. Puigmartí-Luis and S. Pané, MOFBOTS: metal–organic-framework-based biomedical microrobots, *Adv. Mater.*, 2019, **31**, 1901592.

17 J. Liu, J. Li, G. Wang, W. Yang, J. Yang and Y. Liu, Bioinspired zeolitic imidazolate framework (ZIF-8) magnetic micromotors for highly efficient removal of organic pollutants from water, *J. Colloid Interface Sci.*, 2019, **555**, 234–244.

18 H. Luo, Y. Han, K. Hu, J. Li, D. H. L. Ng, X. Ma, K. Luan and M. Yang, Synthesis of dual function Fe_3O_4@MnO_2@HKUST-1 magnetic micromotors for efficient colorimetric detection and degradation of hydroquinone, *New J. Chem.*, 2023, **47**, 1094–1104.

19 H. K. Kim, W. S. Yun, M.-B. Kim, J. Y. Kim, Y.-S. Bae, J. Lee and N. C. Jeong, A chemical route to activation of open metal sites in the copper-based metal–organic framework materials HKUST-1 and Cu-MOF-2, *J. Am. Chem. Soc.*, 2015, **137**, 10009–10015.

20 G. Majano and J. Pérez-Ramírez, Scalable room-temperature conversion of copper(II) hydroxide into HKUST-1 ($Cu_3(btc)_2$), *Adv. Mater.*, 2013, **25**, 1052–1057.

21 J. Du, C. Zhang, H. Pu, Y. Li, S. Jin, L. Tan, C. Zhou and L. Dong, HKUST-1 MOFs decorated 3D copper foam with superhydrophobicity/superoleophilicity for durable oil/water separation, *Colloids Surf., A*, 2019, **573**, 222–229.

22 V. Stavila, J. Volponi, A. M. Katzenmeyer, M. C. Dixon and M. D. Allendorf, Kinetics and mechanism of metal–organic framework thin film growth: systematic investigation of HKUST-1 deposition on QCM electrodes, *Chem. Sci.*, 2012, **3**, 1531–1540.

23 Q. Li, W. Zhu, Y. Lian, Y. Peng and Z. Deng, One-dimensional HKUST-1 nanobelts from Cu nanowires, *Chin. Chem. Lett.*, 2020, **31**, 517–520.

24 A. A. Mashentseva, A. L. Kozlovskiy and M. V. Zdorovets, Electrochemical template synthesis of copper nanotubes from nitrate and sulfate electrolytes, *Russian J. Gen. Chem.*, 2019, **89**, 988–993.

25 D. Collins, T. Luxton, N. Kumar, S. Shah, V. K. Walker and V. Shah, Assessing the impact of copper and zinc oxide nanoparticles on soil: a field study, *PLoS One*, 2012, **7**, e42663.

26 S. Han, R. A. Ciufo, M. L. Meyerson, B. K. Keitz and C. B. Mullins, Solvent-free vacuum growth of oriented HKUST-1 thin films, *J. Mater. Chem. A*, 2019, **7**, 19396–19406.

27 S. Han, R. A. Ciufo, B. R. Wygant, B. K. Keitz and C. B. Mullins, Methanol oxidation catalyzed by copper nanoclusters incorporated in vacuum-deposited HKUST-1 thin films, *ACS Catal.*, 2020, **10**, 4997–5007.

28 K. Yuan, V. de la Asunción-Nadal, B. Jurado-Sánchez and A. Escarpa, 2D Nanomaterials wrapped janus micromotors with built-in multiengines for bubble, magnetic, and light driven propulsion, *Chem. Mater.*, 2020, **32**, 1983–1992.

29 V. de la Asunción-Nadal, B. Jurado-Sánchez, L. Vázquez and A. Escarpa, Magnetic fields enhanced the performance of tubular dichalcogenide micromotors at low hydrogen peroxide levels, *Chem. – Eur. J.*, 2019, **25**, 13157–13163.

30 J. R. Álvarez, E. Sánchez-González, E. Pérez, E. Schneider-Revueltas, A. Martínez, A. Tejeda-Cruz, A. Islas-Jácome, E. González-Zamora and I. A. Ibarra, Structure stability of HKUST-1 towards water and ethanol and their effect on its CO_2 capture properties, *Dalton Trans.*, 2017, **46**, 9192–9200.

31 A. Terracina, M. Todaro, M. Mazaj, S. Agnello, F. M. Gelardi and G. Buscarino, Unveiled the source of the structural instability of HKUST-1 powders upon mechanical compaction: definition of a fully preserving tableting method, *J. Phys. Chem. C*, 2019, **123**, 1730–1741.

32 C. Li, A. Chandresh, Z. Zhang, S. Moulai and L. Heinke, Stability and degradation of metal–organic-framework films under ambient air explored by uptake and diffusion experiments, *Adv. Mater. Interfaces*, 2022, **9**, 2101947.

33 K.-S. Lin, A. K. Adhikari, C.-N. Ku, C.-L. Chiang and H. Kuo, Synthesis and characterization of porous HKUST-1 metal organic frameworks for hydrogen storage, *Int. J. Hydrogen Energy*, 2012, **37**, 13865–13871.